The 5th European sCO2 Conference for Energy Systems
March 14-16, 2023, Prague, Czech Republic

2023-sCO2.eu-112

INFLUENCE OF THE EQUATION OF STATE ON THE DESIGN OF SCO2-POWER CYCLES

Sebastian Rath*
TU Dresden
Dresden, Germany
Email: sebastian.rath@tu-dresden.de

Uwe Gampe
TU Dresden
Dresden, Germany

Andreas Jäger
TU Dresden
Dresden, Germany

ABSTRACT

The favorable location of the critical point close to common ambient temperatures makes carbon dioxide (CO_2) highly attractive to be used as working fluid for supercritical power cycles. The combination of the thereby wide usable range of temperatures with the special fluid properties close to the critical point, e.g. high densities and low viscosities, holds a distinctive potential for significant efficiency increases as well as smaller component sizes compared to the actual state of the art. However, due to the highly non-ideal behavior of the fluid properties in the regions of interest, especially at near-critical conditions, reliable equations of state (EoS) are needed to correctly predict the fluid behavior. This concerns all steps in design and development of supercritical power cycles, from the preliminary modeling of the cycle up to tasks of detailed engineering of individual components. If, in addition, mixtures or impurities are considered instead of a pure substance, the deviation of the EoS of each component is also included in the mixture calculation, which underlines the importance of accurate EoS. Therefore, a certain sensitivity is required to what extent the selection of the EoS may influence the expected results.
In this work, the influence of different equations of state on the thermodynamic design of CO_2 power cycles is investigated. Within this context, five different equations of state were compared to each other by calculating a selection of power cycle configurations, which are typically considered for sCO_2 applications. Aside characteristic process parameters such as relevant fluid properties at each state point of the cycle and the thermal efficiency, differences in the sizes for the internal heat exchangers are considered.
The results show, with some exceptions, a largely good agreement in the cycle efficiencies for most of the considered EoS. However, it can also be seen, that the thermophysical properties can differ significantly between the EoS, which is also reflected in notable variations in the heat exchanger performance parameters and furthermore may lead to non-negligible deviations in subsequent evaluations.

INTRODUCTION

The critical point of CO_2 at a pressure of $p_c = 73.773$ bar and a temperature of $\vartheta_c = 30.9782$ °C, which is quite close to ambient conditions, facilitates the use of carbon dioxide (CO_2) as working fluid for supercritical power cycles for a variety of applications. Compared to the actual state-of-the-art, i.e., steam Rankine cycles and gas turbine Brayton cycles, sCO_2 holds a distinctive potential for significant efficiency increases as well as smaller component sizes. Current investigations range from the preliminary modeling of the cycle including thermoeconomic studies [1,2], detailed engineering of individual components [3], up to the selective admixing of dopants in order to influence selected target values [4–6].
However, due to the highly non-ideal behavior of the fluid properties in the regions of interest, especially at near-critical conditions, reliable equations of state (EoS) are needed to correctly predict the fluid behavior. The resulting effects on the design parameters of power cycles have so far received only limited attention.

Zhao et al. [7] has compared selected EoS for a rather simple recuperated cycle investigating six different equations of state. They concluded that concerning cycle efficiency, the influence of different equations of state is not as significant as for other properties, which are important for designing components, as for example the UA-coefficient of heat exchangers. These findings are in line with investigations of Rath et al. [5,6] who used

* corresponding author(s)

DOI:10.17185/duepublico/77268

different mixture models for modeling a simple cycle as well as a recuperated cycle with sCO_2 as working fluid and the findings of Mickoleit et al. [8] for a split air conditioner with internal heat exchanger. In the aforementioned works, different mixture models and their results have been compared and it was found that the influence of the equations of state on the thermal efficiency as well as on the COP was rather limited whereas other properties, such as the UA-coefficient, differ more significantly when using different equations of state. However, regarding the usage of sCO_2, mostly the influence of equations of state on rather simple cycle architectures with only limited technical relevance has been investigated in the literature.

Therefore, the purpose of this work is to extend these considerations to more complex cycle configurations, which are commonly discussed for sCO_2 power cycles. Herein, emphasis is placed on the actual impact of different frequently used equations of state on the overall design values of various cycle configurations. Related to the frequent use of even simpler equations of state, it is intended to raise awareness of the importance of a proper selection on exemplary base of the selected commonly discussed cycle architectures. The studied equations of state comprise the Soave-Redlich-Kwong equation of state (SRK), the Peng-Robinson equation of state (PR), the Lee-Kesler-Plöcker equation of state (LKP), the PCP-SAFT equation of state, as well as the actual reference equation of state for CO_2 by Span and Wagner [9].

EQUATIONS OF STATE

In order to compare the influence of the equations of state (EoS) on various performance parameters of thermodynamic cycles, such as thermal efficiency, and the UA value as a performance parameter for the heat exchangers, different equations of state have been used in this work. The software TREND 5.0 [10] has been used for the calculation of thermophysical properties. The studied equations of state, which are available in the software TREND, are the Soave-Redlich-Kwong equation of state (SRK) [11,12], the Peng-Robinson equation of state (PR) [13], the Lee-Kesler-Plöcker equation of state (LKP) [14,15], the PCP-SAFT equation of state [16–20], and multiparameter equations of state, i.e., the reference equation for CO_2 by Span and Wagner [9] formulated in the dimensionless Helmholtz energy α. The used models will be briefly introduced in the following.

Multiparameter equations of state formulated in the dimensionless Helmholtz energy α can be considered the state-of-the-art in accurate property modeling. These equations of state are empirical in nature and are typically capable of representing all experimental data within the experimental uncertainty of the measurements. The dimensionless Helmholtz energy α is commonly split into an ideal part α^0, representing the dimensionless Helmholtz of the ideal gas and a residual part α^r, accounting for the real behavior of the substance. It is

$$\frac{a}{RT} = \alpha(\tau,\delta) = \alpha^0(\tau,\delta) + \alpha^\mathrm{r}(\tau,\delta). \quad (1)$$

In Eq. (1), τ denotes the reciprocal reduced temperature

$$\tau = T_\mathrm{c}/T \quad (2)$$

and δ the reduced density

$$\delta = \rho/\rho_\mathrm{c}. \quad (3)$$

with T_c and ρ_c being the critical temperature and critical density of the substance, respectively. T denotes the temperature and ρ the molar density in Eqs. (2) and (3). The ideal part α^0 can be obtained from experimental (or simulated) data for the isobaric heat capacity of the ideal gas and the ideal gas law. The residual part consists of empirical terms, commonly referred to as polynomial-like terms, exponential terms, Gaussian-bell shaped terms, and non-analytical terms. The reference equation of state by Span and Wagner [9] consists of 42 of these terms.

The cubic equations of state, i.e., the SRK and PR, are implemented in TREND as described by Bell and Jäger [21]. When translating the SRK to the residual dimensionless Helmholtz energy, it reads

$$\alpha^\mathrm{r} = -\ln(1-b\delta\rho_\mathrm{c}) - \frac{\tau a}{RT_\mathrm{c}}\frac{\ln(b\rho_\mathrm{c}\delta+1)}{b}. \quad (4)$$

The PR translated to the residual dimensionless Helmholtz energy becomes

$$\alpha^\mathrm{r} = -\ln(1-b\delta\rho_\mathrm{c}) - \frac{\tau a}{RT_\mathrm{c}}\frac{\ln\left(\frac{\left(1+\sqrt{2}\right)b\rho_\mathrm{c}\delta+1}{\left(1-\sqrt{2}\right)b\rho_\mathrm{c}\delta+1}\right)}{2\sqrt{2}b}. \quad (5)$$

In Eqs. (4) and (5), a is the attraction parameter and b the co-volume of the SRK and PR, respectively. Details for the calculation of a and b can be found in, e.g., [21].

The basic idea of the LKP is to interpolate the compression factor z of the fluid of interest using the compression factor of a simple fluid (methane, argon, krypton) z^0 with an acentric factor of $\omega^0 = 0$ and the compression factor of a reference fluid (n-octane) z^r with an acentric factor of $\omega^\mathrm{r} = 0.3978$. The LKP reads

$$z = z^0 + \frac{\omega}{\omega^\mathrm{r}}(z^\mathrm{r} - z^0). \quad (6)$$

The implementation of the LKP in TREND is described in the work of Herrig [22]. The application of the SRK, PR, and LKP for CO_2 only requires the critical properties as well as the acentric factor. The values used in this work are listed in Table 1.

Table 1: Critical properties and acentric factor of CO_2 used for the SRK, PR, and LKP in this work

ω	T_c/K	p_c/MPa
0.224	304.1282	7.3773

Finally, the PCP-SAFT equation of state for CO_2 reads

$$a^{\mathrm{r}} = a^{\mathrm{hc}} + a^{\mathrm{disp}} + a^{\mathrm{QQ}}, \tag{7}$$

where the hard-chain term and the dispersion term are given in Ref. [18] and the quadrupole-quadrupole interaction term is given by Ref. [19]. The parameters for the PCP-SAFT equation of state used for CO_2 in this work are given in Table 2

Table 2: Parameters for the PCP-SAFT equation used for CO_2 in this work

m	σ/Å	$(\varepsilon/k_{\mathrm{B}})$/K	Q/DÅ
1.5131	3.1869	163.33	4.4

All of the equations of state used in this work are implemented in TREND according to the form given in Eq. (1). The residual parts of the Helmholtz energy for the SRK, PR, LKP, and PCP-SAFT are given in Eqs. (4)-(7). The ideal part of the dimensionless Helmholtz energy α^0 can be obtained by integrating over the ideal gas isobaric heat capacity c_p^0. For the multiparameter equation of state, the correlation for α^0 given by Span and Wagner [9] has been used. For all other equations of state, c_p^0 have been calculated with a correlation given in the VDI-Wärmeatlas [23], which reads

$$\frac{c_p^0}{R} = B + (C-B)\left(\frac{T}{A+T}\right)^2 \cdot \left[1 - \frac{A}{A+T}\left(D + E\frac{T}{A+T} + F\left(\frac{T}{A+T}\right)^2 + G\left(\frac{T}{A+T}\right)^3\right)\right]. \tag{8}$$

The parameters for Eq. (8) are given in Table 3

Table 3: Parameters for the ideal gas isobaric heat capacity of CO_2 according to Eq. (8)

A	B	C	D	E	F	G
514.5073	3.4923	–0.9306	–6.0861	54.1586	–97.5157	70.9687

Thermophysical properties of CO_2 can be calculated from Eq.(1) by combining the dimensionless Helmholtz energy and its derivatives with respect to the independent variables τ and ρ. For example, it is [24]

$$p = \rho RT\left(1 + \delta\left(\frac{\partial\alpha^{\mathrm{r}}}{\partial\delta}\right)_{\tau}\right), \tag{9}$$

$$h = RT\left[1 + \tau\left(\frac{\partial\alpha^0}{\partial\tau}\right)_{\delta} + \tau\left(\frac{\partial\alpha^{\mathrm{r}}}{\partial\tau}\right)_{\delta} + \delta\left(\frac{\partial\alpha^{\mathrm{r}}}{\partial\delta}\right)_{\tau}\right], \tag{10}$$

and

$$s = R\left[\tau\left(\frac{\partial\alpha^0}{\partial\tau}\right)_{\delta} + \tau\left(\frac{\partial\alpha^{\mathrm{r}}}{\partial\tau}\right)_{\delta} - \alpha^0 - \alpha^{\mathrm{r}}\right]. \tag{11}$$

Note that in Eqs. (9), (10), and (11) the intensive variables ρ, h, s are molar if the universal gas constant R is used and these variables are specific, if the specific gas constant is used.

CYCLE MODELING

To evaluate the influence of the EoS, four supercritical cycle architectures of varying complexity were selected, which have also been considered frequently in recent literature for various applications of sCO_2 power cycles.

The simple recuperated cycle (SRC) represents the most basic configuration of recuperated supercritical Brayton cycles. Compared to the non-recuperated cycle, it promises high efficiencies with a manageable number of components, so that it is often chosen as a basis for investigations in related topics as well as for comparison with cycles of higher complexity (e.g., [25]). As shown in Figure 1, the SRC includes the essential main components to represent a recuperated Brayton cycle. Starting at the compressor inlet in point 1, the fluid is compressed to the upper pressure level. Subsequently, heat is added in the recuperator (2 to 3) and the heater (3 to 4) until the turbine inlet temperature is reached in point 4. After expansion to the lower pressure level in point 5, excess heat is rejected by passing the recuperator (5 to 6) and the cooler (6 to 1) going back to starting conditions. However, one drawback of this simple layout is a certain limitation of the amount of recuperable heat caused by the strong variation of the near critical heat capacities and the resulting mismatch in the temperature changes of the hot and the cold side. To counteract this effect, the recompression cycle (RCC) divides the heat recovery into two separate recuperators, a high temperature unit (HTR) and a low temperature unit (LTR) including a split in the mass flow in between at the cold side (point 8). While the main flow passes the cooler (8 to 1), the main compressor (1 to 2) and the LTR (2 to 3), the second stream bypasses the cooler and gets compressed in a re-compressor (8 to 3) without prior heat rejection, rejoining the main flow at the outlet of the LTR in point 3. In this way, the heat capacity flows in the LTR can be adjusted to prevent the aforementioned mismatch in temperatures. Subsequently, the rejoined mass flow passes the HTR (3 to 4) and the heater until it reaches the turbine inlet temperature (TIT) in point 5 and finally gets expanded in the turbine to the lower pressure level at the inlet of the HTR in point 6. Since with appropriately selected bypass mass flows the re-compressor work input is less than the heat removed in the cooler, higher thermal efficiencies can be achieved compared to the SRC architecture [26].

To further improve the thermal efficiency, the RCC can be expanded to more complex layouts, such as the intercooled cycle (ICC) or the partial cooling cycle (PCC), which are also taken into account in this work. As shown on the bottom left in Figure 1, in the intercooled cycle (ICC) the compression of the main fluid flow is split up to two stages, namely the pre-compressor (9 to 10) and the main compressor (1 to 2). Within this configuration, the fluid rejects heat in an intercooler at intermediate pressure (10 to 1), before entering the main-

DOI: 10.17185/duepublico/77268

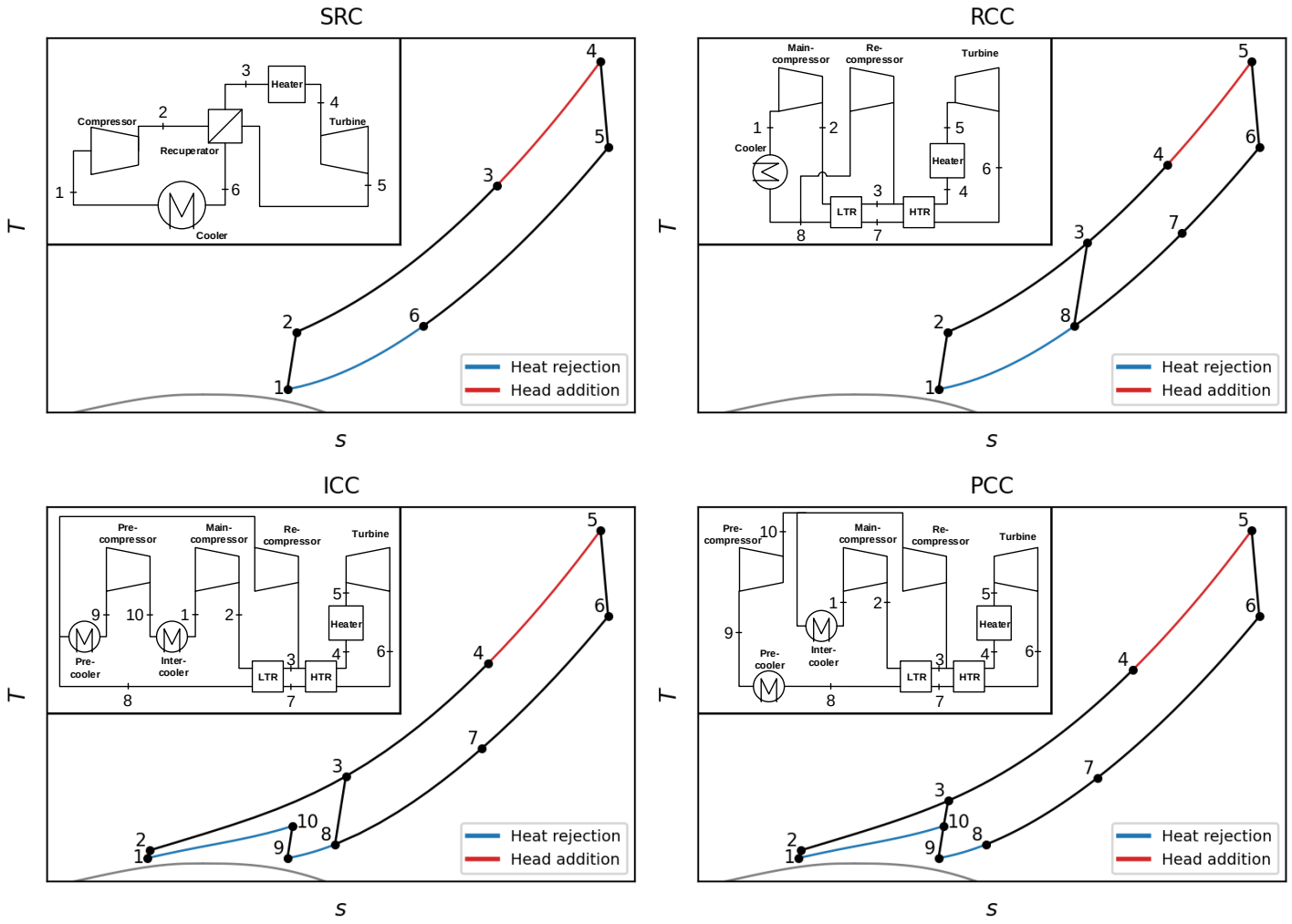

Figure 1: *T-s* diagrams and block-layouts of the considered cycle architectures

compressor. This leads to a reduced total compressor work and thus to higher efficiencies [27].

Related to this, the concept of a staged compression is also taken up in the precooled cycle (PCC), shown at the bottom right of Figure 1. Starting at the low pressure side exit of the LTR in point 8, the whole mass flow passes a pre-cooler (8 to 9) and pre-compressor (9 to 10). Subsequently, the split-up takes place at intermediate pressure. Whereas the bypass flow directly gets compressed by the re-compressor (10 to 3), heat is rejected again from the main flow in an intercooler (10 to 1) before entering the main compressor (1 to 2).

Using the equations of state described before, calculations were done for all four layouts based on a set of preset values for the inlet of the main compressor, the turbine inlet as well as the mass-flow bypass ratio and the intermediate pressure level for the higher order cycles.

To take account for the strong variation of the flow properties, a step-wise approach was chosen for all recuperators by splitting up the device into multiple segments of constant enthalpy change (cf. Figure 2). Then, the evaluation was done iteratively by setting a minimum pinch point difference (ΔT_R). Starting from an assumed initial value, e.g. $T_6 = T_2 + \Delta T_\mathrm{R}$ in the SRC, the guess is iteratively adjusted until the pinch-point criterion is met in all sections.

Herein, the UA value is determined for each recuperator as the product of the heat transfer coefficient U and the heat exchanger area A. The UA value is a common metric for initial classification of heat exchanger size and performance, widely used in common literature, also for sCO_2 applications, e.g. [28–30].

Based on the heat flux given by the enthalpy differences of the fluid on each side it can be calculated by:

$$UA = \frac{\dot{Q}}{\mathrm{LMTD}} \tag{12}$$

DOI: 10.17185/duepublico/77268

As no explicit values for the mass flows are set within the thermodynamic analysis of the cycles, and since the absolute values are not relevant for a relative comparison of the EoS within one cycle architecture, a relative formulation for the mass flow is used. Assuming a constant heat input for each cycle, the EoS-specific, relative mass-flow can be calculated by relating the value of the enthalpy difference in the heater for each EoS to the value gained by using the reference equation. This results in:

$$m^* = \frac{h_4 - h_3}{h_{4,\mathrm{ref}} - h_{3,\mathrm{ref}}} \tag{13}$$

for the simple recuperated cycle, and

$$m^* = \frac{h_5 - h_4}{h_{5,\mathrm{ref}} - h_{4,\mathrm{ref}}} \tag{14}$$

for all other cycle configurations. Consequently, in combination with Eqs (12) this results in:

$$UA = \frac{\dot{Q}}{\mathrm{LMTD}} = \frac{\Delta h_\mathrm{R} \cdot m^*}{\mathrm{LMTD}} \tag{15}$$

In Eqs. (12) and (13), LMTD is the mean log temperature difference given by:

$$\mathrm{LMTD} = \frac{\Delta T_\mathrm{hot} - \Delta T_\mathrm{cold}}{\ln(\Delta T_\mathrm{hot}) - \ln(\Delta T_\mathrm{cold})} \tag{16}$$

With ΔT_hot and ΔT_cold referring to the temperature differences at the hot and cold side of the recuperator, respectively. With regard to the previously mentioned segment-based approach, the *UA* value for the entire device, as shown in Figure 2, arises as the sum of the *UA* values of the individual segments:

$$\mathrm{UA_{tot}} = \sum_{i=1}^{n} \mathrm{UA}_i = \sum_{i=1}^{n} \frac{\Delta h_i \cdot m^*}{LMTD_i} \tag{17}$$

Alternatively, the same result can be obtained by using the averaged logarithmic temperature difference of all segments:

$$\mathrm{UA_{tot}} = \frac{\Delta h_\mathrm{R} \cdot m^*}{\overline{LMTD}} \tag{18}$$

With $\overline{LMTD}$ calculated as the harmonic mean of the individual values of all segments:

$$\overline{LMTD} = \frac{n}{\sum_{i=1}^{n} LMTD_i^{-1}} \tag{19}$$

In equations (17) and (19) *n* refers to the total number of sections. As shown in Figure 2 on an exemplary division into 12 sections and in contrast to the conventional calculation of the heat exchanger as a single section, this allows a better consideration of the changes in the fluid properties and the resulting non-linearity of the temperature lines, which finally leads to a more accurate value for *UA*. In the calculations performed here, the recuperators were divided into 24 segments each.

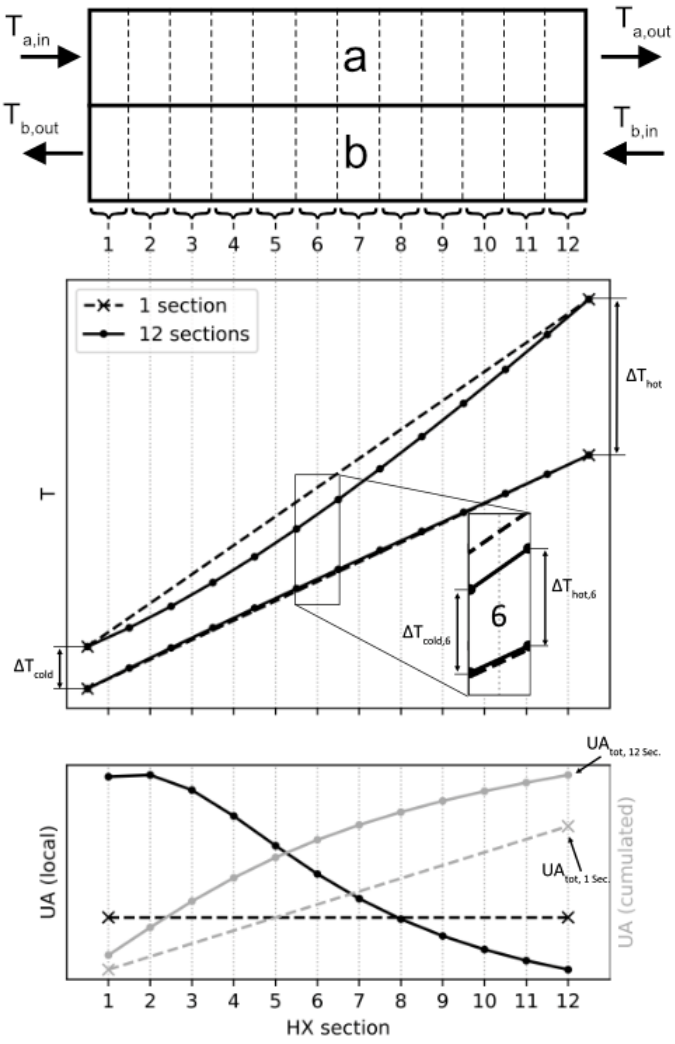

Figure 2: Illustration of the segment-wise evaluation of the *UA* value for better consideration of non-ideal (non-linear) fluid properties, including, going through from top to bottom, the schematic segmentation of the heat exchanger, the resulting differences in the temperature lines, and the resulting differences in the local and cumulated values for *UA*. In both plots, for *T* as well as for *UA*, the dashed line refers to the non-segmented (1 segment) approach and the solid line referring to the split up of the device into 12 sections.

As a second parameter to compare the EoS, the thermal efficiency was used which generally can be calculated by relating the heat rejected from the cycle to the cycles heat input:

$$\eta_\mathrm{th} = 1 - \frac{\left|\dot{Q}_\mathrm{out}\right|}{\dot{Q}_\mathrm{in}} \tag{20}$$

DOI: 10.17185/duepublico/77268

Related to the cycle architectures described above, this leads to

$$\eta_{\mathrm{th,SRC}} = 1 - \frac{h_6 - h_1}{h_4 - h_3} \tag{21}$$

for the simple recuperated cycle, to

$$\eta_{\mathrm{th,RCC}} = 1 - \frac{(h_8 - h_1) \cdot (1 - m_{\mathrm{BR}})}{h_5 - h_4} \tag{22}$$

for the recompression cycle, to

$$\eta_{\mathrm{th,ICC}} = 1 - \frac{(h_8 - h_9 + h_{10} - h_1) \cdot (1 - m_{\mathrm{BR}})}{h_5 - h_4} \tag{23}$$

for the intercooling cycle, and to

$$\eta_{\mathrm{th,PCC}} = 1 - \frac{(h_{10} - h_1) \cdot (1 - m_{\mathrm{BR}}) + (h_8 - h_9)}{h_5 - h_4} \tag{24}$$

for the partial cooling cycle. Herein, in Equations (22) to (24), m_{BR} is the fractional amount of bypassed mass-flow.

The boundary conditions applied to the thermodynamic cycles are listed in Table 4. Temperatures were oriented to an exemplary waste heat recovery application, i.e., acting as a bottoming cycle using the exhaust heat from a gas turbine process. Thus, the higher temperature level, directly corresponding to the turbine inlet temperature, is set to a fixed value of TIT = 550°C which is in the range of typical gas-turbine exhaust temperatures (c.f. Glos et al. [31]). The lower temperature is varied within a range of 32 °C to 40 °C regarding to different recooling conditions. The lower pressure level is set to a near critical value of 7.4 MPa while the higher pressure level is set to 25 MPa corresponding to a typical value for sCO_2 cycles. The intermediate pressure level for the intercooled cycle and the precooled cycle was set arbitrarily to 8.5 MPa. Similarly, the fractional amount of bypassed mass-flow was set to a value of 0.2. Losses were treated in terms of isentropic efficiencies for the compressor and the turbine. For the recuperators, a minimum pinch point difference of $\Delta T_{\mathrm{R}} = 10\ \mathrm{K}$ was applied. Pressure losses were completely neglected.

Table 4: Boundary conditions applied to the process calculations

Boundary condition	Symbol	Value
Minimum temperature	$\vartheta_{\mathrm{low}} \equiv \mathrm{CIT_{mc}}$	35 °C (32 .. 40 °C)
Maximum temperature	$\vartheta_{\mathrm{high}} \equiv \mathrm{TIT}$	550 °C
Lower pressure level	p_{low}	7.5 MPa
Upper pressure level	p_{high}	25 MPa
Intermediate pressure (ICC, PCC)	p_{mid}	8.5 MPa
Mass-flow bypass ratio	m_{BR}	0.2
Compressor efficiency	η_{C}	0.8
Turbine efficiency	η_{T}	0.9
Min. pinch point diff. recuperator	ΔT_{R}	10 K

NEAR CRITICAL MODELING CAPABILITIES OF THE SELECTED EQS

For an initial cycle-independent comparison of the near-critical capabilities of the selected equations of state, several sets of isobars were calculated for relevant fluid properties in a temperature range close to critical conditions.

Beginning with the plots for the isobaric heat capacity, shown in Figure 3, it can be seen that all EoS are able to show the general behavior of a peak in the properties flattening with increasing distance from the critical pressure, including its shifts towards higher temperatures. However, compared to the multi-parameter equation of state, all other equations partly show a clear offset from the reference values. Focusing on the cubic equations of state (PR, SRK) and PCP-SAFT, these EoS predict the heat capacity peak at significantly lower temperatures than the other equations of state, resulting in higher values for c_{p} for temperatures below the pseudocritical point and lower values for temperatures above. Furthermore, the same EoS show notably lower peaks at higher pressure levels. The trend to lower values continues for higher temperatures, showing only slow convergence to the reference values. In contrast, the LKP shows a comparatively good agreement with the reference equation for the near-critical 7.4 MPa isobar. Nevertheless, for temperatures below the pseudocritical point and higher pressures, obtained values for c_p are clearly below the reference.

A somewhat similar behavior can be seen for the isobars in the ρ-T diagram shown in Figure 4. Especially the cubic equations as well as PCP-SAFT show remarkably lower values for the density with increasing differences to the reference EoS for higher pressures. In contrast, also here, the LKP shows good agreement with the reference values on all isobars with only

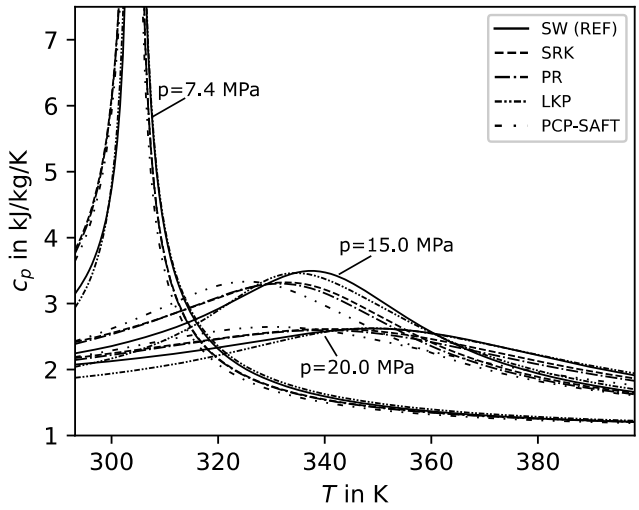

Figure 3: Near critical isobaric heat capacities for several isobars calculated with the selected EoS

DOI: 10.17185/duepublico/77268

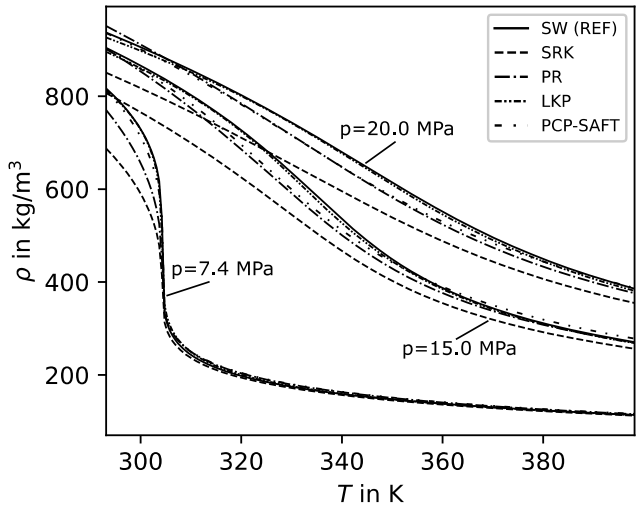

Figure 4: Near critical densities for several isobars calculated with the selected EoS

small deviations. Moreover, for the heat capacity as well as for the density, all equations of state converge to ideal gas behavior at higher temperatures. As expected, at higher pressures the results converge slower to the ideal gas limit, i.e. the differences in the results of the equations of state tend to be greater at greater pressure at the same temperature.

RESULTS AND DISCUSSION

In order to compare the influence of the selected EoS, calculations were done for all four cycle architectures regarding the boundary conditions specified in Table 4 and for an initially fixed lower temperature level of 35 °C. The results for each equation of state are listed in Table 5 in terms of calculated values for the reference EoS by Span and Wagner and related to this, the percentage relative deviation for all other EoS is given.
Starting with the thermal efficiencies, it can be seen that for all cycles all EoS show a fairly good agreement with each other. The largest differences compared to the reference equation are found in the results for the cubic equations and for the usage of PCP-SAFT. Herein, it can be seen that the SRK leads to higher deviations in the efficiency for the simpler layouts (SRC, RCC) than for the more complex cycle architectures (ICC, PCC). PCP-SAFT, on the other hand, shows smaller deviations in the results for the SRC and RCC than for the efficiencies of higher order cycles examined here.
In contrast to the efficiencies, the results for *UA* partially show large differences between the individual equations of state. In case of the cubic equations of state (SRK, PR), deviations from the reference EoS of up to 23.3 % can be observed in the results for the high-temperature recuperator of the RCC. Significant differences can also be seen for the application of PCP-SAFT, ranging from about -4 % for the low-temperature recuperator (LTR) of the PCC up to over 40 % for the high-temperature recuperator (HTR) of the RCC. In contrast, also here, the results

Table 5: Relative deviation of the calculated values compared to the reference equation of state

			Relative deviation from the reference value in % $100 \cdot \left(\frac{x - x_{\mathrm{REF}}}{x_{\mathrm{REF}}}\right)$			
		SW (ref)	SRK	PR	LKP	PCP-SAFT
SRC	η_{th}	0.377	-1.056 %	0.2089 %	-0.243 %	1.136 %
	m^*	1.0	1.223 %	1.565 %	-1.902 %	3.322 %
	UA_R	8.16	6.513 %	8.847 %	-2.370 %	13,550 %
	Δh_R	313.77	0.701 %	0.508 %	0.380 %	-1.713%
	$\overline{LMTD}_R$	38.44	-4.300 %	-6.843 %	0.862 %	-10.566 %
RCC	η_{th}	0.398	-1.260 %	0.240 %	-0.309 %	1.088 %
	m^*	1.0	1.418 %	1.582 %	-1.846 %	3.288 %
	UA_{LTR}	11.57	10.716 %	14.400 %	-1.886 %	25.408 %
	Δh_{LTR}	229.25	-0.162 %	-1.277 %	2.217 %	-3.058 %
	$\overline{LMTD}_{LTR}$	19.92	-8.667 %	-12.505 %	2.261 %	-20.410 %
	UA_{HTR}	4.50	14.214 %	23.274 %	-9.846 %	40.360 %
	Δh_{HTR}	130.37	2.102 %	3.281 %	-2.207 %	0.612 %
	$\overline{LMTD}_{HTR}$	29.00	-9.336 %	-14.893 %	6.470 %	-25.962 %
ICC	η_{th}	0.413	-0.308 %	1.050 %	0.108 %	2.335 %
	m^*	1.0	3.366 %	4.068 %	-0.373 %	5.423 %
	UA_{LTR}	9.89	-2.634 %	4.775 %	1.883 %	8.080 %
	Δh_{LTR}	250.57	-1.232 %	-2.934 %	1.147 %	-5.498 %
	$\overline{LMTD}_{LTR}$	25.35	-0.527 %	-3.589 %	-1.093 %	-7.821 %
	UA_{HTR}	3.07	14.189 %	22.463 %	-1.479 %	33.785 %
	Δh_{HTR}	179.49	-2.282 %	-0.972 %	-2.741 %	0.453 %
	$\overline{LMTD}_{HTR}$	58.41	-11.544 %	-15.847 %	-1.650 %	-20.843 %
PCC	η_{th}	0.400	-0.531 %	0.733 %	-0.076 %	2.171 %
	m^*	1.0	2.196 %	2.970 %	-1.037 %	4.978 %
	UA_{LTR}	6.43	-10.156 %	-9.635 %	-3.973 %	-3.912 %
	Δh_{LTR}	113.18	-12.995 %	-14.896 %	-6.559 %	-11.094 %
	$\overline{LMTD}_{LTR}$	17.60	-1.034 %	-3.026 %	-3.703 %	-2.868 %
	UA_{HTR}	4.63	12.806 %	17.972 %	2.787 %	23.400 %
	Δh_{HTR}	289.40	1.797 %	2.026 %	1.146 %	0.057 %
	$\overline{LMTD}_{HTR}$	62.46	-7.778 %	-10.948 %	-2.617 %	-14.977 %

DOI: 10.17185/duepublico/77268

of the LKP show much smaller deviations from the results of the reference equation of state. Most of them are in the single-digit percentage range. The highest value with approx. 10 % is obtained again for the high-temperature recuperator of the RCC.

In comparison with the previously discussed results for the near-critical heat capacities in Figure 3, it is noticeable that equations of state, which show significant offsets in the heat capacities, also lead to significant deviations for the calculated UA values of the recuperators. Taking the 15 MPa isobar in Figure 3 as an example, a clear offset to lower values can be seen for both the cubic equations of state as well as for PCP-SAFT. In addition, the less pronounced shift of the LKP also coincides with the lower deviations in the calculated values for UA in Table 5. However, a closer look at the deviations of the individual variables associated with the calculation of UA (cf. Equation (15)), which are also listed in Table 5, reveals different influences on the final value for UA. Starting with m^*, which indicates the relative change in the mass-flow regarding the reference equation, for the cubic equations as well as for the PCP-SAFT equation deviations in a positive single digit percentage range can be noted for all cycle architectures. The LKP, on the other hand, shows small negative deviations between −1.9 % and approx. −0.4 % in each case. Herein, it is noticeable, that increased values for m^* are not necessarily linked with increased values for UA. For instance, in the case of the ICC, the use of the LKP results in a slightly reduced mass flow rate, but still an increased value for UA.

A contrasting example can be found for the cubic equations of state applied to the pre-compression cycle (PCC), in which higher relative mass flows m^* result in lowered values in the UA values for the low-temperature recuperator (LTR) but in elevated ones for the high-temperature unit (HTR). Moreover, for all cycle architectures, the largest deviations in mass flow occur when using the PCP-SAFT equation.

In contrast, a more distinct influence on UA can be found in the deviations for the mean logarithmic temperature differences ($\overline{LMTD}$), cf. equation (19), as well as for the enthalpy difference Δh between in- and outlet of each device. In case of the simple recuperated cycle and the recompression cycle, also Δh shows only smaller deviations in small single digit percentage ranges. Noticeable higher deviations can be seen for $\overline{LMTD}$ instead, being in line with the order of magnitude of the deviations in UA. For example, the previously mentioned 40 % increase in UA for the high-temperature recuperator of the RCC when using PCP-SAFT results in a deviation of about −26 % in $\overline{LMTD}$, but only 0.612 % in Δh (and approx. 3.3 % in m^*). Similar results can be found for the usage of the cubic EoS for both cycle architectures. The results using the LKP are less significant in this aspect, since the deviations, for UA as well as for Δh and $\overline{LMTD}$, are much less pronounced than for the other equations of state.

However, especially when looking at the results of the cubic EoS, effects change partially in case of the ICC and the PCC, depending on the temperature level of the recuperator. While the aforementioned prevalence in the deviation in $\overline{LMTD}$ is mainly

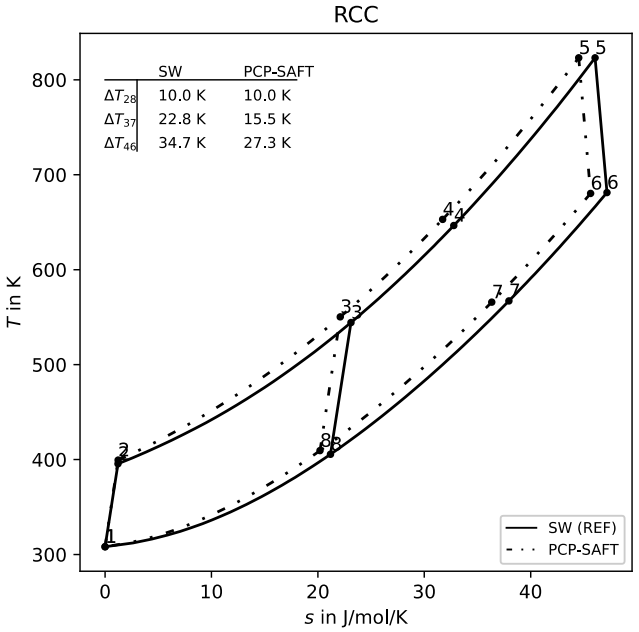

Figure 5: *T-s* diagram of the RCC on base of different EoS, including a comparison of the terminal temperature differences of both recuperators

evident for the HTR, relative values for $\overline{LMTD}_{\mathrm{LTR}}$ and Δh_{LTR} are quite close to each other regarding the ICC, up to the case that Δh_{LTR} shows up remarkable higher deviations than $\overline{LMTD}_{\mathrm{LTR}}$ for the PCC. With reference to the latter, for example, deviations in UA for the low temperature recuperator are about −10 %, whereas relative deviations for Δh_{LTR} are around 13 % (SRK) to 15 % (PR) while $\overline{LMTD}_{LTR}$ deviates only in a range from

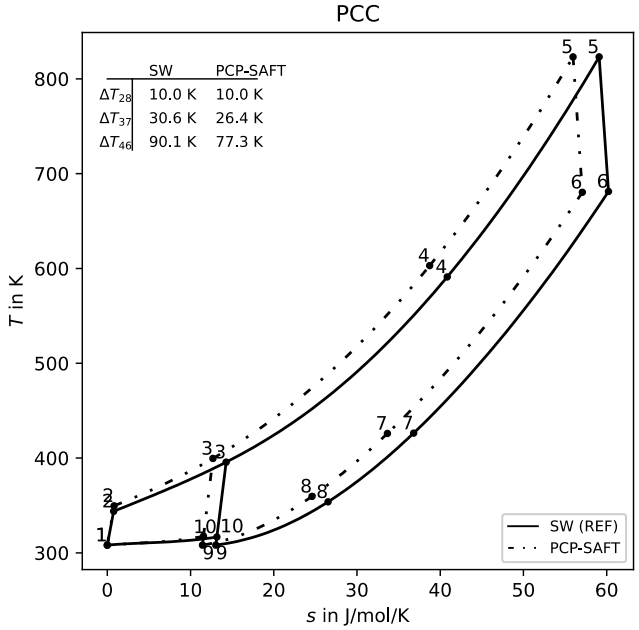

Figure 6: *T-s* diagram of the PCC on base of different EoS, including a comparison of the terminal temperature differences of both recuperators

DOI: 10.17185/duepublico/77268

approximately −1 % (SRK) to −3 %. Similarly, the same can be noted for the PCP-SAFT and the LKP, although, as before, the effect is less pronounced in case of the LKP equation due to the generally smaller deviations from the reference equation.

Based on the case with the largest deviation in the calculated values for UA, Figure 5 shows the T-s diagram of the recompression cycle on the one hand calculated with the reference equation by Span and Wagner and on the other hand calculated with PCP-SAFT using the boundary conditions from Table 4 in each case.
Referring to the aforementioned trend to lower values in the isobaric heat capacities for PCP-SAFT, a faster increase in temperature compared to the reference EoS can be seen, i.e., the isobar of the PCP-SAFT EoS exhibits a steeper slope than the isobar of the reference EoS in a T-s diagram.
The comparison of the temperature differences of the state points, corresponding to the terminal temperature differences of the recuperators (c.f. top left in Figure 5) shows that this leads to lower temperature differences in the recuperators, which, in accordance with Eqs. (12) and (13), result in higher values for UA. Moreover, the mutual influence of the recuperators in the higher order cycles leads to a potential multiplication of the deviation within the calculation process by using the result from the preceding component (e.g. LTR) as a boundary condition for the subsequent component (e.g. HTR).
Additionally, Figure 6 shows the same comparison of T-s diagrams calculated with the reference EoS and with PCP-SAFT

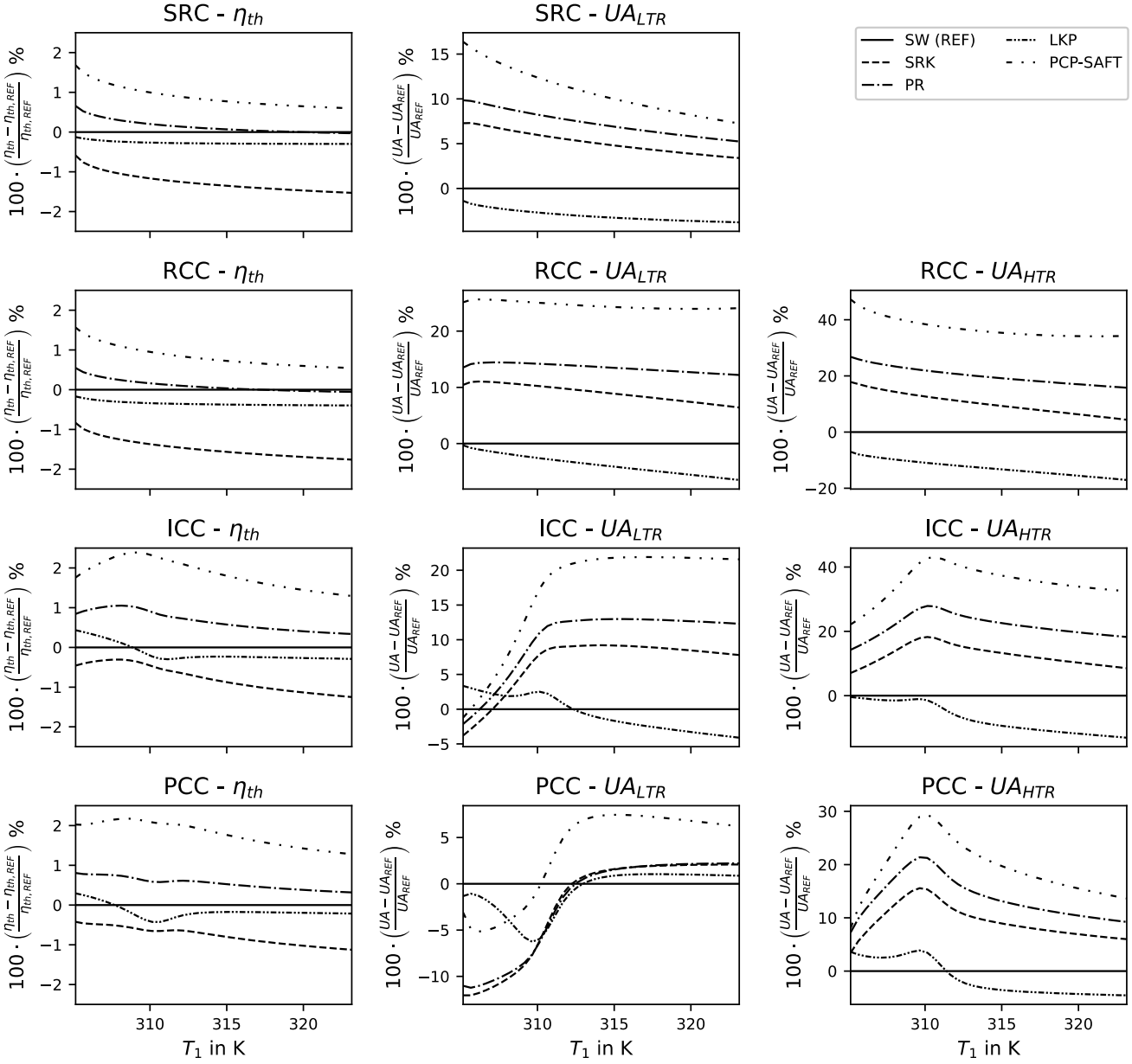

Figure 7: Changes in the relative deviation of the calculated properties for varying compressor inlet temperatures

DOI: 10.17185/duepublico/77268

for the precompression cycle (PCC) and the boundary condition specified in Table 4. As before, the PCP-SAFT equation shows a faster increase in temperature compared to the reference EoS resulting in a shift of the state points and respective changes in the terminal temperature differences of the recuperators. However, it can also be seen that, due to the lower temperature at the compressor outlet in point 2, the temperature range of the LTR (approx. 350 K to 400 K) is significantly lower than in case of the RCC (approx. 400 K to 540 K). Taking again into account the curves for the isobaric heat capacities in Figure 3, it can be noted, that for the higher pressure levels significantly larger deviations in the heat capacity are to be expected in this temperature range. Using the example of the 20 MPa isobar, it is apparent, that this clearly covers the range of the pseudocritical peak of the fluid properties. This in turn infers, that the significantly increased heat capacity in this region combined with the EoS specific shifts in the pseudocritical point itself, leads to the previously noted more prevalent deviations in the enthalpy differences Δh_{LTR} compared to changes in the temperature resulting in deviations of $\overline{LMTD}_{\mathrm{LTR}}$

Finally, Figure 7 shows the changes in the deviations of $\eta_{\mathrm{th}}$and UA for varying compressor inlet temperatures, as specified within the boundary conditions in Table 4. It can be seen that for the cases considered here, even with reference to a wider temperature range, the deviations in efficiency remain within a small range of $\pm$ 2.5 %. Beyond that, it is noticeable that the usage of the SRK consistently results in lower efficiencies compared to SW, while using PR and PCP-SAFT mostly yields values above the reference

Regarding the UA values, the results underline the dependency on the capabilities of the EoS to model supercritical heat capacities. Thus, for values of c_p well below the reference at higher temperatures (c.f. Figure 3), as is the case for SRK, PR, and PCP-SAFT, comparably high positive deviations in the UA values of up to over 40 % can be seen. Although the compressor inlet temperature only allows limited statements to be made about the recuperator inlet conditions, it can be further assumed, that the change to negative deviations of UA, especially visible for the low temperature recuperator in the ICC and the PCC, for lower values of T_1 relates to the offset in the heat capacity peak to lower temperatures. Analogous to the efficiencies, a certain tendency towards stabilized values for the deviations can also be seen here for higher temperatures. Nevertheless, the deviations remain at fairly high values.

CONCLUSION

In summary, in this work the influence of different EoS on the calculation of efficiency and heat exchanger performance of several power cycle architectures frequently considered for applications with sCO_2 as working fluid has been studied. Within this context, five different equations of state were compared to each other. For the calculated efficiencies, even the results of the simpler equations of state show an overall good agreement with the reference values. Nevertheless, especially for more complex cycle architectures deviations in a single-digit percentage range may occur, which may not be negligible for more detailed evaluations. However, it has also been shown that the choice of the EoS is even more significant when it comes to the calculation of components. Based on the example of the UA value, as a widely used performance and size indicator for heat exchangers, deviations in the values for the recuperators of more than 40 % were noticed. Note that the observed differences in the results of the cycle calculations with the equations of state studied in this work do not reflect the deviations of the different EoS at the same state points but are a result of error propagation, since the different EoS lead to different state points at the inlets and outlets of the components as discussed in Figure 5 and Figure 6. However, the deviations are exclusively due to the use of a different EoS, i.e., there are no other influences which could explain the observed differences.

Both, the good agreement of the calculated efficiencies as well as the deviations found in the calculated values for UA are in good agreement with the findings of Mickoleit et al. [8] or Zhao [7], which underlines the importance of the use of an appropriate EoS also beyond the scope of the cycles considered here. This becomes especially important if mixtures are considered as working fluids, because usually the reference equation of state (multiparameter equation of state) is used to calculate the base case. Therefore, it is favorable to also use the reference equation of state in the mixture model in order to get consistent results, as the use of other equations of state might result in significant deviations for performance parameters of the cycle as demonstrated in this work.

NOMENCLATURE

Symbols

a	molar Helmholtz energy (J mol^{-1})
	attraction parameter (Pa m^6 mol^{-2})
A	area (m^2)
b	co-volume (m^3 mol^{-1})
h	molar enthalpy (J mol^{-1})
	specific enthalpy (J kg^{-1})
i	counting variable for summation (-)
k_{B}	Boltzmann constant (J K^{-1})
$LMTD$	logarithmic mean temperature difference (K)
$\dot{m}$	mass flow (kg/s)
m^*	relative mass flow factor (kg/s)
n	number of sections (-)
p	pressure (Pa)
Q	quadrupole moment (DÅ $= 3.3356 \cdot 10^{40}$ Cm^2)
R	universal gas constant
s	molar entropy (J mol^{-1} K^{-1})
	specific entropy (J kg^{-1} K^{-1})
T	temperature (K)
U	heat transfer coefficient (W m^{-2} K^{-1})
UA	UA value as the product of U and A (W K^{-1})
z	compression factor (-)

DOI: 10.17185/duepublico/77268

Greek symbols

α	dimensionless Helmholtz energy (-)
δ	reduced density (-)
ε	segment energy parameter (J)
η	efficiency (-)
ϑ	temperature (°C)
ρ	molar density (mol m^{-3})
	specific density (kg m^{-3})
σ	segment size parameter (Å)
τ	reciprocal reduced temperature (-)

Subscripts

1 .. 10	related to the corresponding process point
BR	bypass ratio (fractional amount of the bypassed mass-flow)
c	property at the critical point
HTR	related to the high-temperature recuperator
LTR	related to the low temperature recuperator
mc	related to the main compressor
t	related to the turbine
th	thermal, related to the (thermal) efficiency
R	related to the recuperator
ref	related to the reference (EoS)

Superscripts

0	ideal gas property
r	residual property

Chemical Formulas

CO_2	carbon dioxide

Abbreviations

CIT	(main-) compressor inlet temperature
EoS	equation of State
HTR	high temperature recuperator
ICC	intercooling cycle
LMTD	logarithmic mean temperature difference
LTR	low temperature recuperator
PR	Peng-Robinson equation of state
PCP-SAFT	perturbed-chain polar Statistical associating fluid theory
PCC	partial cooling cycle
RCC	recompression cycle
SRC	simple recuperated cycle
SRK	Soave-Redlich-Kwong equation of state
SW	multi-parameter EoS by Span and Wagner
TIT	turbine inlet temperature

ACKNOWLEDGEMENTS

This work was carried out within the Supercritical Carbon Dioxide-Lab (suCOO-Lab) of the School of Engineering Sciences of TU Dresden. The authors want to thank the School of Engineering Sciences of TU Dresden for partial funding of the presented results.

REFERENCES

[1] T. Gotelip, U. Gampe, S. Glos, Optimization strategies of different SCO_2 architectures for gas turbine bottoming cycle applications, Energy. 250 (2022) 123734. https://doi.org/10.1016/j.energy.2022.123734.

[2] G. Manzolini, M. Binotti, D. Bonalumi, C. Invernizzi, P. Iora, CO2 mixtures as innovative working fluid in power cycles applied to solar plants. Techno-economic assessment, Solar Energy. 181 (2019) 530–544. https://doi.org/10.1016/j.solener.2019.01.015.

[3] S. Unger, J. Müller, M.B. Mohankumar, S. Rath, U. Hampel, Numerical Dimensioning of a Pre-Cooler for sCO_2 Power Cycles to Utilize Industrial Waste Heat, Energies. 14 (2021) 8278. https://doi.org/10.3390/en14248278.

[4] M. Binotti, C.M. Invernizzi, P. Iora, G. Manzolini, Dinitrogen tetroxide and carbon dioxide mixtures as working fluids in solar tower plants, Sol. Energy. 181 (2019) 203–213. https://doi.org/10.1016/j.solener.2019.01.079.

[5] S. Rath, E. Mickoleit, U. Gampe, C. Breitkopf, A. Jäger, Study of the influence of additives to CO_2 on the performance parameters of a sCO_2-cycle, in: Proceedings of the 4th European SCO2 Conference for Energy Systems, Online-Conference, 2021. https://doi.org/10.17185/duepublico/73965.

[6] S. Rath, E. Mickoleit, U. Gampe, C. Breitkopf, A. Jäger, Systematic analysis of additives on the performance parameters of sCO_2 cycles and their individual effects on the cycle characteristics, Energy. 252 (2022) 123957. https://doi.org/10.1016/j.energy.2022.123957.

[7] Q. Zhao, M. Mecheri, T. Neveux, R. Privat, J.-N. Jaubert, Selection of a Proper Equation of State for the Modeling of a Supercritical CO_2 Brayton Cycle: Consequences on the Process Design, Ind. Eng. Chem. Res. 56 (2017) 6841–6853. https://doi.org/10.1021/acs.iecr.7b00917.

[8] E. Mickoleit, C. Breitkopf, A. Jäger, Influence of Equations of State and Mixture Models on the Design of a Refrigeration Process, Int. J. Refrig. 121 (2021) 193–205. https://doi.org/10.1016/j.ijrefrig.2020.10.017.

[9] R. Span, W. Wagner, A New Equation of State for Carbon Dioxide Covering the Fluid Region from the Triple-Point Temperature to 1100 K at Pressures up to 800 MPa, J. Phys. Chem. Ref. Data. 25 (1996) 1509–1596. https://doi.org/10.1063/1.555991.

[10] R. Span, R. Beckmüller, S. Hielscher, A. Jäger, E. Mickoleit, T. Neumann, S.M. Pohl, B. Semrau, M. Thol, TREND. Thermodynamic Reference and Engineering Data 5.0, (2020).

[11] O. Redlich, J.N.S. Kwong, On the Thermodynamics of Solutions. V. An Equation of State. Fugacities of Gaseous Solutions., Chem. Rev. 44 (1949) 233–244. https://doi.org/10.1021/cr60137a013.

[12] G. Soave, Equilibrium Constants from a Modified Redlich-Kwong Equation of State, Chem. Eng. Sci. 27 (1972) 1197–1203. https://doi.org/10.1016/0009-2509(72)80096-4.

DOI: 110.17185/duepublico/77268

[13] D.-Y. Peng, D.B. Robinson, A New Two-Constant Equation of State, Ind. Eng. Chem. Fund. 15 (1976) 59–64. https://doi.org/10.1021/i160057a011.
[14] B.I. Lee, M.G. Kesler, A Generalized Thermodynamic Correlation Based on Three-Parameter Corresponding States, AIChE J. 21 (1975) 510–527. https://doi.org/10.1002/aic.690210313.
[15] U. Plöcker, H. Knapp, J. Prausnitz, Calculation of High-Pressure Vapor-Liquid Equilibria from a Corresponding-States Correlation with Emphasis on Asymmetric Mixtures, Ind. Eng. Chem. Process Des. Dev. 17 (1978) 324–332. https://doi.org/10.1021/i260067a020.
[16] W.G. Chapman, G. Jackson, K.E. Gubbins, Phase equilibria of associating fluids: Chain molecules with multiple bonding sites, Mol. Phys. 65 (1988) 1057–1079. https://doi.org/10.1080/00268978800101601.
[17] W.G. Chapman, K.E. Gubbins, G. Jackson, M. Radosz, New Reference Equation of State for Associating Liquids, Ind. Eng. Chem. Res. 29 (1990) 1709–1721. https://doi.org/10.1021/ie00104a021.
[18] J. Gross, G. Sadowski, Perturbed-Chain SAFT: An Equation of State Based on a Perturbation Theory for Chain Molecules, Ind. Eng. Chem. Res. 40 (2001) 1244–1260. https://doi.org/10.1021/ie0003887.
[19] J. Gross, An equation-of-state contribution for polar components: Quadrupolar molecules, AIChE J. 51 (2005) 2556–2568. https://doi.org/10.1002/aic.10502.
[20] J. Gross, J. Vrabec, An equation-of-state contribution for polar components: Dipolar molecules, AIChE J. 52 (2006) 1194–1204. https://doi.org/10.1002/aic.10683.
[21] I.H. Bell, A. Jäger, Helmholtz Energy Transformations of Common Cubic Equations of State for Use with Pure Fluids and Mixtures, J. Res. Natl. Inst. Stan. 121 (2016) 238–263. https://doi.org/10.6028/jres.121.011.
[22] S. Herrig, New Helmholtz-energy equations of state for pure fluids and CCS-relevant mixtures, Dissertation, Ruhr-Universität Bochum, 2018. https://hss-opus.ub.ruhr-uni-bochum.de/opus4/frontdoor/deliver/index/docId/6284/file/diss.pdf (accessed February 7, 2019).
[23] Verein Deutscher Ingenieure, VDI-Gesellschaft Verfahrenstechnik und Chemieingenieurwesen, eds., VDI-Wärmeatlas, 11., bearb. und erw. Aufl., Springer Vieweg, Berlin, 2013.
[24] R. Span, Multiparameter Equations of State: An Accurate Source of Thermodynamic Property Data, Springer, Berlin, Germany, 2000.
[25] F. Crespi, G. Gavagnin, D. Sánchez, G.S. Martínez, Supercritical carbon dioxide cycles for power generation: A review, Applied Energy. 195 (2017) 152–183. https://doi.org/10.1016/j.apenergy.2017.02.048.
[26] A. Moisseytsev, J.J. Sienicki, Performance improvement options for the supercritical carbon dioxide brayton cycle., 2008. https://doi.org/10.2172/935094.
[27] J. Yin, Q. Zheng, Z. Peng, X. Zhang, Review of supercritical CO2 power cycles integrated with CSP, Int J Energy Res. 44 (2020) 1337–1369. https://doi.org/10.1002/er.4909.
[28] T. Held, J. Miller, D. Buckmaster, A Comparative Study of Heat Rejection Systems for sCO2 Power Cycles, in: San Antonio, Texas, USA, 2016.
[29] S.-I. Na, M.S. Kim, Y.-J. Baik, M. Kim, Optimal allocation of heat exchangers in a Supercritical carbon dioxide power cycle for waste heat recovery, Energy Conversion and Management. 199 (2019) 112002. https://doi.org/10.1016/j.enconman.2019.112002.
[30] J.S. Kwon, S. Son, J.Y. Heo, J.I. Lee, Compact heat exchangers for supercritical CO2 power cycle application, Energy Conversion and Management. 209 (2020) 112666. https://doi.org/10.1016/j.enconman.2020.112666.
[31] S. Glos, M. Wechsung, R. Wagner, A. Heidenhof, D. Schlehuber, Evaluation of sCO2 power cycles for direct and waste heat applications, (2018). https://doi.org/10.17185/DUEPUBLICO/46082.

DOI: 10.17185/duepublico/77268

DOI: 10.17185/duepublico/77268
URN: urn:nbn:de:hbz:465-20230427-104755-5